DOI: https://doi.org/10.24425/amm.2025.153501

A. SHARMA [1*], S.CH. KUNDURTI [1], R.S. BURADAGUNTA [2], S. SINGH [3], P. TAMBE [1]

ANALYSIS OF MECHANICAL PROPERTIES AND MICROSTRUCTURAL DEVELOPMENT IN Al_2O_3/rGO AND hBN/rGO REINFORCED AA6061-T6 SURFACE COMPOSITES VIA FRICTION STIR PROCESSING

In the current work, the surface of AA6061-T6 alloy has been modified by friction stir processing (FSP) to assess microstructural development and mechanical behaviour. The grooves were made on the surface of the base alloy to deposit the reinforcements (Al_2O_3 + rGO), and (hBN + rGO) thus one pass was made with the probeless tool to pack the reinforcements into the groove, and 2 more passes in the same direction to compactly fabricate the FSPed composites. The fabricated specimens showed a decreased grain size along with the uniformly dispersed reinforcements in the stir zone (SZ) which can be observed in the microstructural studies. Furthermore, the altered intensity of the significant X-ray Diffraction (XRD) peaks was observed in the FSPed composites which indicates the reinforced elements as evidence of the uniform dispersion. In comparison of the reinforced elements, the Al_2O_3 + rGO hybrid reinforcement showcased better results of electrical conductivity and thermal conductivity than the hBN + rGO hybrid reinforcement but a slight reduction when compared to the base alloy AA6061-T6. Increased microhardness of 14.86% and tensile strength of 4.39% with an increase of ductility of 8.64% for hBN + rGO hybrid reinforcement was observed when compared to the Al_2O_3 + rGO hybrid reinforcement. The impact test was conducted for all the surface composites revealed a significant increase of 8.3% in load absorbing capacity with the hybrid reinforcements hBN + rGO compared to the Al_2O_3 + rGO reinforcement. These results suggest the promising role of modifying base alloy with surface reinforcements via FSP to improve the material performance.

Keywords: Aluminum alloy; surface reinforcement; FSP; microstructural characterization; mechanical properties

1. Introduction

Materials engineering has long recognized aluminum alloys as versatile materials owing to their excellent combination of mechanical properties, i.e. lightweight nature, high strength-to-weight ratio, corrosion resistance, thermal conductivity, electrical conductivity, ease of fabrication, and recyclability [1-2]. These properties make aluminum alloys a versatile choice for industrial applications such as aerospace, automotive, marine, and electronics, where performance, efficiency, and sustainability are utmost important [3]. Yet, in specific instances, the poor wear resistance and hardness of some materials may limit their use [4]. Introducing ceramic nanoparticles, e.g. SiC, Al_2O_3, ZrO_2, GNP, B_4C, Gr, SiO_2, etc., by FSP into aluminum alloys has greatly altered the microstructural and mechanical characteristics [5-7]. In recent years, the use of FSP has emerged as a transformative method for improving the properties and functionalities of aluminum alloys by fabricating surface composites [8-9]. FSP enables the fabrication of surface composites by locally heating and stirring the material under the action of a rotating tool [10-11]. By operating at temperatures below the materials' melting point, FSP minimizes thermal deformation and preserves the integrity of both the base material and reinforcement, unlike conventional melting processes [12].

Abbass et al. [13] studied the improvement in microhardness (89.3%) and slightly better wear resistance of AA6061-T6 by incorporating SiC and Al_2O_3 ceramic particles via FSP. Ammal et al. [14] also studied the improvement in the microhardness (130%) and better tensile properties of AA6061-T6 by the incorporation of ZrO_2-GNP hybrid reinforcement particles via FSP. Yunus et al. [15] revealed the improvement of compression strength (22%) better than the base material (BM) AA6061-T6 by incorporation of the B_4C and Gr hybrid reinforcement particles into the matrix via dual stir casting technique. Sharma et al. [16] found an average increment of hardness of 32% when they utilized different strategies for incorporating hybrid reinforcements of B_4C+MoS_2 into the BM AA6061. Mengstie et al. [17] focuses on optimizing the process parameters for FSP to

[1] SCHOOL OF MECHANICAL ENGINEERING, VIT-AP UNIVERSITY, AMARAVATI, ANDHRA PRADESH, INDIA-522237
[2] DEPARTMENT OF MECHANICAL ENGINEERING, COLLEGE OF ENGINEERING, PRINCE MOHAMMAD BIN FAHD UNIVERSITY, AL KHOBAR 31952, SAUDI ARABIA
[3] DEPARTMENT OF MECHANICAL ENGINEERING, TSINGHUA UNIVERSITY, BEIJING 100084, CHINA

* Corresponding author: sharma.ambuj@vitap.ac.in

fabricate a surface composite by reinforcing agate particles into AA6061-T6 aluminum alloy. Suman et al. [18] investigate the impact of silicon carbide particles on the temperature distribution, microstructural evolution, and mechanical properties during the FSP of AA6061-T6 aluminum alloy plates. The study aims to understand how SiC, a widely used ceramic reinforcement, influences the composite's performance when incorporated into the aluminum matrix using FSP. Ali et al. [19] found that an equal amount 7.5 wt.% of SiO_2 and B_4C ceramic reinforcement particles into the BM AA6061-T6 processed via FSP has attained an improvement in the microhardness (155 Hv) when compared to the parent metal (65 Hv). Using reinforcing materials to produce surface composite was the subject of several published investigations. Most of the researchers in the literature focused on examining the effects of variations in the hybrid reinforcement ratio across the FSP [20-27].

This research article investigates the incorporation of Al_2O_3 and hBN nanoparticles, combined with rGO, as hybrid reinforcements for the development of AA6061-T6 surface composites via FSP. The choice of Al_2O_3 and hBN nanoparticles is due to their superior ballistic resistance, while rGO contributes to enhanced mechanical and tribological properties. The primary objective of this study is to assess the effects of this hybrid reinforcement strategy on both the surface and bulk properties of the synthesized SMMCs. This hybrid reinforcement approach opens new opportunities for high-performance applications across various industries. This paper presents a comparative analysis of the reinforcements and examines their substantial impact in comparison to the base metal matrix. Through a detailed analysis of both existing literature and experimental data, this research aims to advance the field of materials and metallurgical engineering by optimizing the performance, efficiency, and sustainability of SMMCs for modern industrial applications.

2. Materials and methods

In this study, AA6061-T6 plates of size $150\times135\times6.35$ mm^3 were procured from Mallinath Metals, India. We cut a 3 mm square groove in the center of the AA6061-T6 plate's surface throughout its length using a CNC end mill cutter. In this study, we procured Al_2O_3 nanopowder particulates, with an average size of 80 nm, and hBN nanopowder particles, with an average size of 100 nm, to serve as reinforcement materials alongside rGO. We used a 10:1 ball-to-powder ratio to ball mill the rGO, which is made up of 5-10 layers with an average lateral dimension of 10 nm, with Al_2O_3 nanopowder in a 1:1 ratio for about 6 hours. We reinforced this ball-milled mixture (Al_2O_3 + rGO) on the AA6061-T6 surface with FSP. The grooves were filled with powders, and surfacing was done using a pinless tool made of tempered H13 tool steel to prevent powder spilling during the processing stage. Next, we processed the plate using a conical thread pin tool, which had a 24 mm shoulder diameter and a 4.7 mm pin length. The pin had a large (7 mm) diameter near the shoulder and a smaller diameter at the other end. It was reported that the lower tool rotational speeds decrease the heat generation and causes poor material flow and higher tool travel speeds allows insufficient time for stirring of material and results in defects in the nugget zone. Hence, selecting an appropriate combination of process parameters is crucial to achieve a defect free stir zone. In the present work, the process parameters to conduct the FSP experiments were selected based on the previous research work literature. For the experiment, a semi-automated milling machine with three axes of control (Model: hmt-three axis servos controlled) was used. It was set to rotate the tool at 1150 rpm, move the table at 50 mm/min, and tilt the tool at 2.5° degrees. One pass with the pin-less tool was passed on the groove surface and two passes with the tapered cylindrical threaded tool was stirred into the packed surface to effectively reinforce the particles into the MMC. Similarly, surface composite reinforced with hBN + rGO was also produced in the same manner. To enhance the mechanical and electrical properties of the SMMCs, a hybrid reinforcement was employed using equal weight percentages of (50% rGO and 50% Al_2O_3) and (50% rGO and 50% hBN). We selected this balanced composition to enhance overall performance and reduce the risk of agglomeration that comes with higher reinforcement concentrations. This method helps the reinforcing particles be spread out more evenly within the matrix, which improves the composite's structural integrity.

We conducted microstructural analysis of the produced surface composites using an optical microscope (OM) (Make: COSLAB CIM100 Inverted Metallurgical Microscope) and a scanning electron microscope (SEM) (Make: ZEISS EVO 10) in accordance with the ASTM E3-95 method [28]. We used abrasive sheets with sizes ranging from 180 to 3000 grit to polish the samples in a progressive fashion. A last step involved fine polishing with diamond paste measuring 0.5 mm [29]. Keller's reagent, consisting of 2 mL of hydrofluoric acid, 3 mL of hydrochloric acid, 5 mL of nitric acid, and 190 mL of distilled water, etched the samples for 30 seconds after polishing them. In order to determine which elements were in the composite, an analytical expert pro conducted the X-ray diffraction (XRD) examination utilizing a RIGAKU MiniFlex machine. The XRD experiments were carried out using CuKα sources ranging from 3 to 90 [30].

We used the Armfield Linear Heat Conduction device, which includes a specimen holder, a heating source, and a set of thermocouples, to measure thermal conductivity. To guarantee complete contact and effective heat exchanges among the various components, the thermal paste was generously coated on all sides. We adjust the cooling water supply flow to the apparatus to 1.5 l/min after timing the collection of 500 ml of water every 20 seconds. Then, the heater is turned on to add heat to the cylinder-heated area. The thermal energy is transferred in a straight path to the sample by passing through a material that is both known and calibrated. In addition, the sample's heat is dispersed as a result of its direct contact with the cooling section, which is made possible by the cooling water supply. The thermal conductivity is directly measured under steady-state circumstances. We conducted an electrical conductivity test on all the manufactured samples using a Keithley 6517B instrument. The Keithley 6517B electrometer is highly accurate, capable of accurately measuring electrical conductivity across a broad range of magnitudes. We conducted quantitative electrical conductivity tests on a minimum of five samples to evaluate its accuracy.

Tensile testing was performed along the FSP direction on the manufactured surface composites. In order to study the tensile behavior of nano-surface composites, tensile specimens were machined from SZ according to ASTM WK49229 – 2015 specifications. These specimens had a 7 mm gauge length, 2.9 mm grip distance, and 4 mm width [31]. Then the testing was carried out using a 10kN capacity universal testing machine (Make: Tinius Olsen H10KL/150) at a strain rate of 0.001/s in ambient environmental conditions. The fractured specimens were further examined by using the SEM to evaluate its behavioural characteristics. The impact test (Make: Digital Impact Testing Machine) was performed on the samples extracted vertically from the SZ following the ASTM E23 standards. The fracture surfaces were examined by using SEM. We conducted a micro-Vickers hardness test (Make: Micro Vickers Hardness tester) on the heat-affected zone (HAZ), base metal (BM), stir zone (SZ), and thermos-mechanically affected zone (TMAZ) of the surface composite, following the ASTM E92-17 criteria [32].

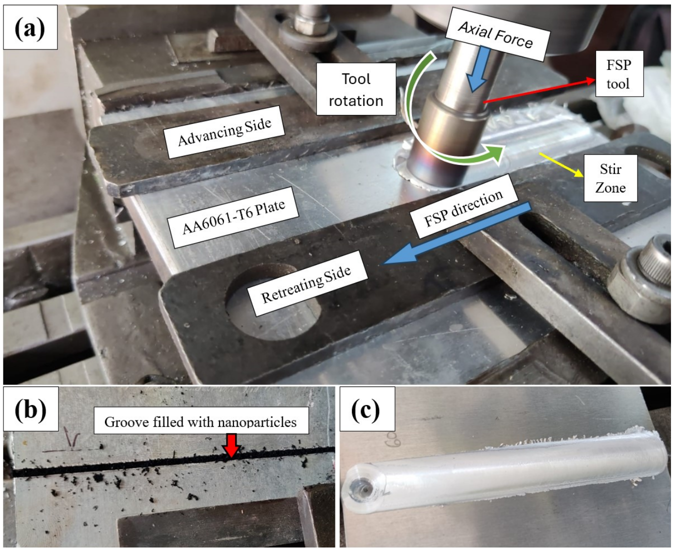

Fig. 1. (a) Schematic representation of the FSP process during the experimentation, (b) Groove filled with nanoparticles, (c) surface reinforced multi-pass FSP processed plate

2. Results and discussions

2.1. Microstructural analysis

Fig. 2 shows how reinforcements changed micrographs of AA6061-T6 alloy taken from different sample cross-sections before and after FSP. The initial microstructure of BM AA6061-T6, shown in Fig. 2(a), consists of elongated grains in a uniaxial direction with an average grain size of 84.2 ± 29.5 μm. FSP resulted

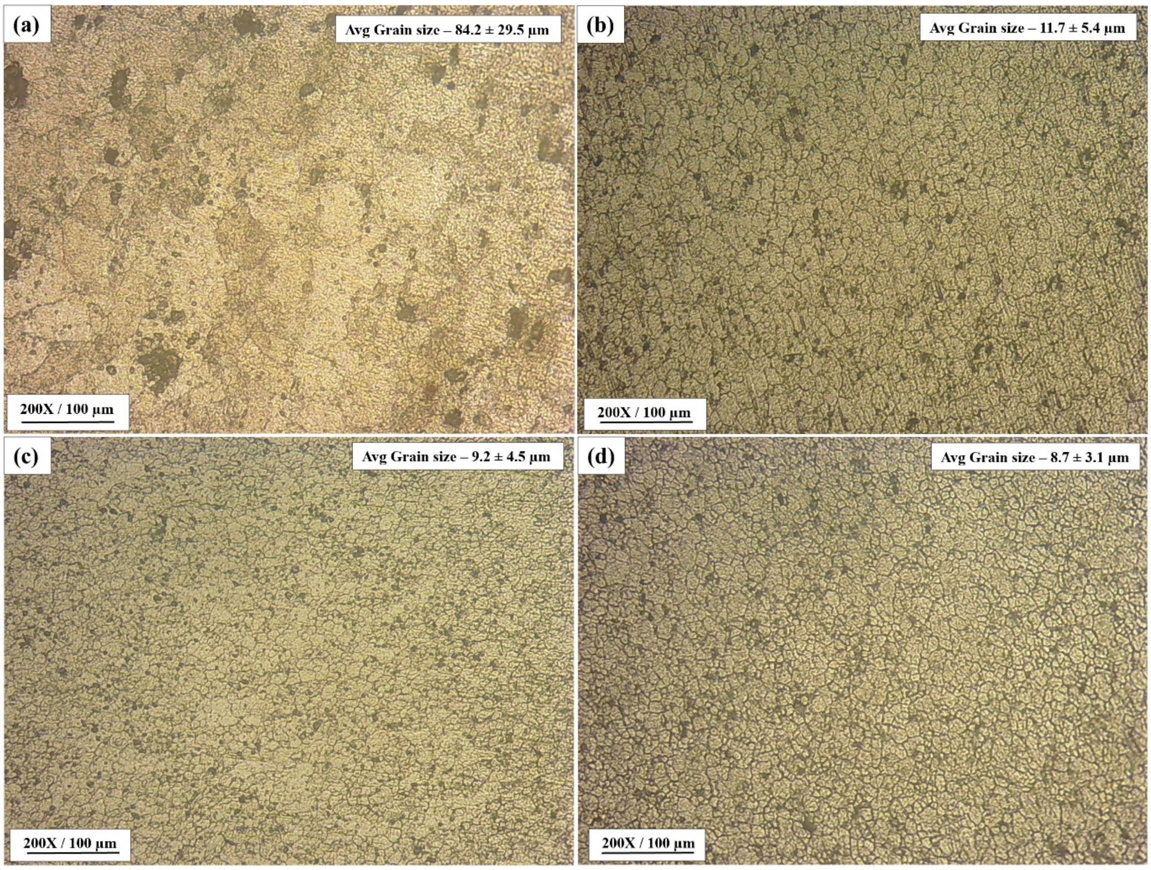

Fig. 2. Optical microstructures of: (a) BM AA6061-T6, (b) FSPed AA6061-T6, (c) AA6061-T6 + (Al_2O_3 + rGO), (d) AA6061-T6 + (hBN + rGO)

in a significant alteration of the microstructure along with a decrease in the grain size of 11.7 ± 5.4 μm, as shown in Fig. 4(b). This is because FSP causes friction and large amounts of plastic deformation, which heats up the SZ and causes a dynamically recrystallized microstructure to form. However, incorporating hybrid reinforcements into the base material further reduced the grain size, indicating that the nanoceramics function as grain refiners, as further evidenced in Fig. 2(c, d). The average grain sizes in the SZ for the hybrid composites AA6061-T6 + (Al_2O_3 + rGO) and AA6061-T6 + (hBN + rGO) were measured as 9.2 ± 4.5 μm and 8.7 ± 3.1 μm respectively. hBN has a hexagonal structure like graphite, which can provide excellent lubrication properties. This lubricating effect can enhance the plastic deformation during FSP, leading to more efficient grain refinement. While Al_2O_3 is harder, and more abrasive compared to hBN. While this can enhance wear resistance, it may also lead to less uniform plastic deformation during FSP, resulting in less effective grain refinement. Also, Al_2O_3 has lower thermal conductivity compared to hBN, which can result in less efficient heat distribution and potentially larger grain sizes. The superior thermal conductivity, lubrication properties, and strong interfacial bonding of hBN primarily contribute to the reduced grain size in AA6061-T6 + (hBN + rGO) compared to AA6061-T6 + (Al_2O_3 + rGO) after FSP. These properties, combined with the nucleation effect of rGO, facilitate more efficient grain refinement. In contrast, the harder and more abrasive nature of Al_2O_3, along with its lower thermal conductivity, results in less effective grain refinement during FSP compared with hBN + rGO reinforcement.

Fig. 3 shows SEM images that demonstrates how the hybrid reinforcement particles (Al_2O_3 + rGO) and (hBN + rGO) are spread out evenly in the alloy matrix after the FSP. The FSP process evenly distributes reinforcing particles while fabricating the surface composite. An equal distribution of reinforcing particles in the surface composite is crucial for excellent mechanical properties. This method disperses reinforcement particles to ensure matrix homogeneity. The homogeneous distribution of reinforcing particles has many benefits. At the outset, incorporating crack prevention barriers improves composite mechanical properties. It prevents large cracks in composite materials, strengthening their structural integrity.

2.2. XRD analysis

The phases present in the BM and the hybrid reinforced FSP treated samples were determined by the XRD analysis. The XRD plots of AA6061-T6 + (hBN + rGO), AA6061-T6 + (Al_2O_3 + rGO), and BM AA6061-T6 are depicted in Fig. 4. It represents the XRD pattern of AA6061-T6, which shows the peaks at 38.72, 44.14, 64.98, 78.04 and 82.00 which correspond to the (111), (200), (220), (311) and (222) planes of Al respectively. These peaks are almost identified in all the reinforced composites also, whereas the additional reinforcements identified at different peaks and planes. For AA6061-T6 + (Al_2O_3 + rGO) having peaks at 40.16, 49.36 and 62.38 corresponds to the (211), (230) and (312) planes of Al_2O_3 and whereas the peaks at 42.19 and 76.10 corresponds to the (104), and (110) planes of C respectively. For AA6061-T6 + (hBN + rGO) having peaks at 42.08 corresponds to the (002) plane of BN and whereas the peaks at 44.85 corresponds to the (111) plane of C respectively.

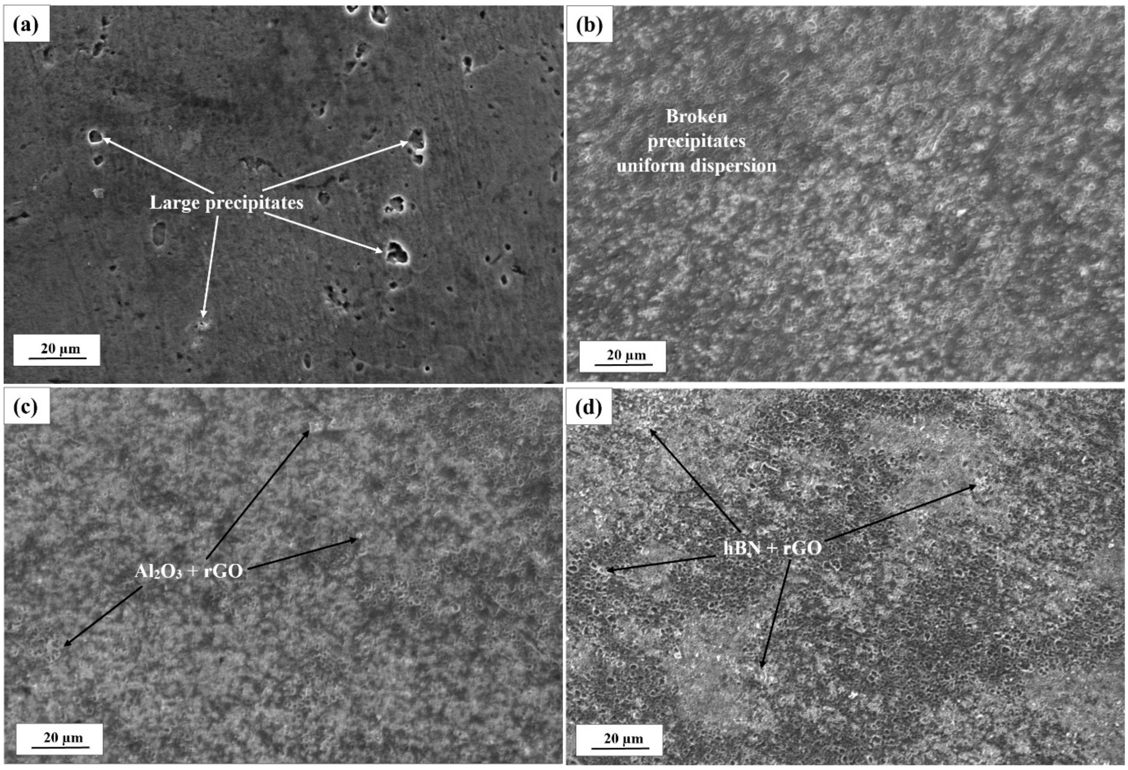

Fig. 3. SEM images of: (a) BM AA6061-T6, (b) FSPed AA6061-T6, (c) AA6061-T6 + (Al_2O_3 + rGO), (d) AA6061-T6 + (hBN + rGO)

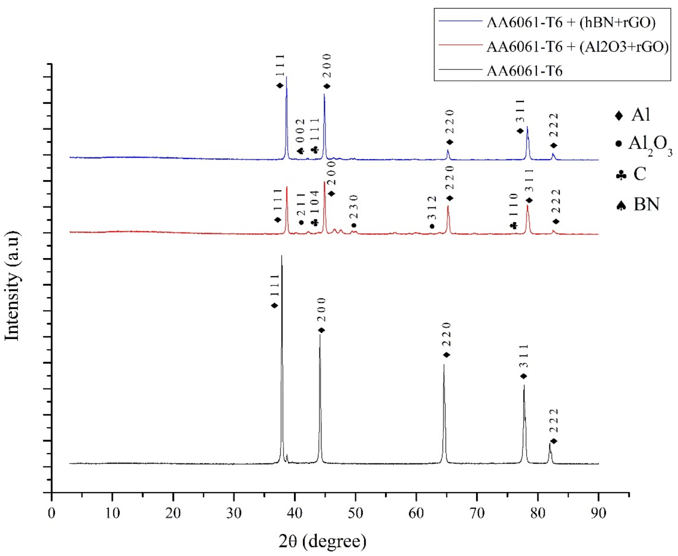

Fig. 4. XRD pattern for all samples

2.3. Electrical conductivity

The electrical conductivity of the AA6061-T6 alloy is estimated to be around 2.71×10^{7} S/m. This study investigated the effects of semiconductor rGO, insulating Al_2O_3, and hBN particles in a composite matrix. Free electrons in rGO facilitate electric current flow, making it more electrically conductive than Al_2O_3 and hBN. Al_2O_3 and hBN are insulators, but rGO is semiconductor. The low band gap of reduced graphene oxide (rGO) promotes electron transport between energy levels. Electron mobility increases electrical conductivity. Additionally, rGO has more free electrons than Al_2O_3 and hBN. This phenomenon occurs because rGO has more valence electrons. The outermost electron shell of an atom contains valence electrons. These electrons carry electricity more easily. Fig. 5 shows that rGO particles improved the aluminum alloy's electrical conductivity, but not as much as the FSPed base metal. The composite material AA6061-T6 + (Al_2O_3 + rGO), had the highest level of electrical conductivity, measuring around 2.1×10^{7} S/m compared to the composite material AA6061-T6 + (hBN + rGO) having a little less electrical conductivity, measuring around 1.925×10^{7} S/m.

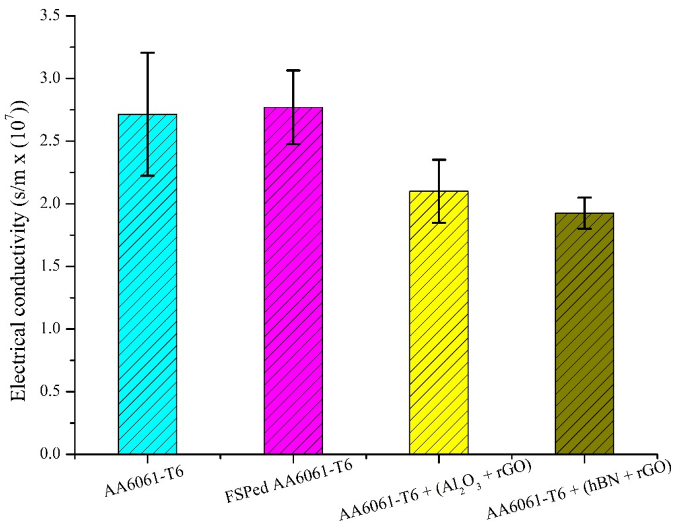

Fig. 5. Electrical Conductivity of all samples

2.4. Thermal conductivity

A substance's thermal conductivity refers to its ability to conduct thermal energy. Thermal conductivity was observed slightly higher in the FSPed AA6061-T6 with 161.41 W/mK when compared to the BM AA6061-T6 with a thermal conductivity of 159.85 W/mK which can be observed in Fig. 6. In fact, the figure shows that the thermal conductivity of metal matrix composites (MMCs) goes down when (Al_2O_3 + rGO) and (hBN + rGO) hybrid reinforcement particles are added, reaching 144.76 W/mK and 142.82 W/mK, respectively. The incorporation of rGO particles into the MMCs can potentially improve the thermal conductivity of the surface MMCs owing to their superior conductive properties. The presence of other insulating elements, such as Al_2O_3 and hBN particles, which possess a higher density than the base matrix, may hinder the heat conductivity of the material.

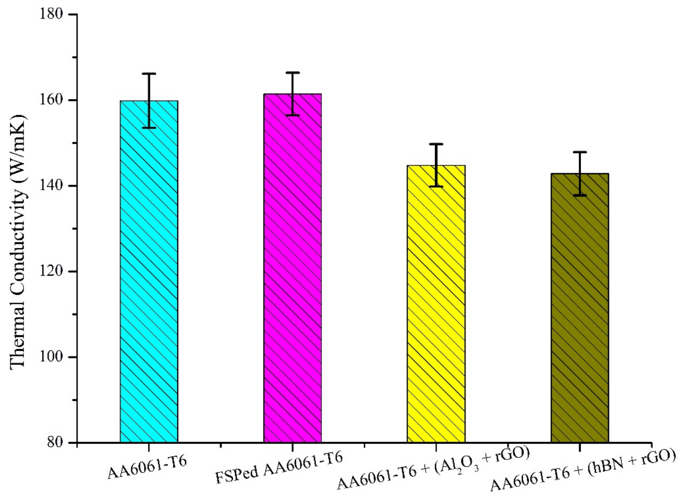

Fig. 6. Thermal Conductivity of all samples

2.5. Mechanical characterization

The effect of FSP and addition of reinforcements into the base material on the mechanical performance are illustrated in Fig. 7. It was evident that the yield strength and UTS of the FSPed and the hybrid reinforced samples were increased to a little extent when compared to the BM AA6061-T6. The hybrid composite with (hBN + rGO) had the highest tensile strength, followed by the (Al_2O_3 + rGO) hybrid composite, FSPed and BM. Both the hybrid composites showed slightly closer strengths and elongation. The increased tensile strength of the hybrid composites is due to the synergistic effects of the two reinforcements. Al_2O_3 and hBN ceramic particles are rigid and brittle substances, whereas rGO is comparatively malleable and resilient. The amalgamation of these two elements can yield a hybrid composite characterized by elevated strength and toughness. The tensile strength improvements of the composites, compared to the BM AA6061-T6, ranged from 16.33% to 11.43%, as illustrated in Fig. 7. According to the results of this study, mixing Al_2O_3 and hBN with rGO reinforcements in hybrid composites has a lot of potential for making materials that are both high-strength and lightweight. These materials are especially appropriate for applications requiring significant strength and toughness.

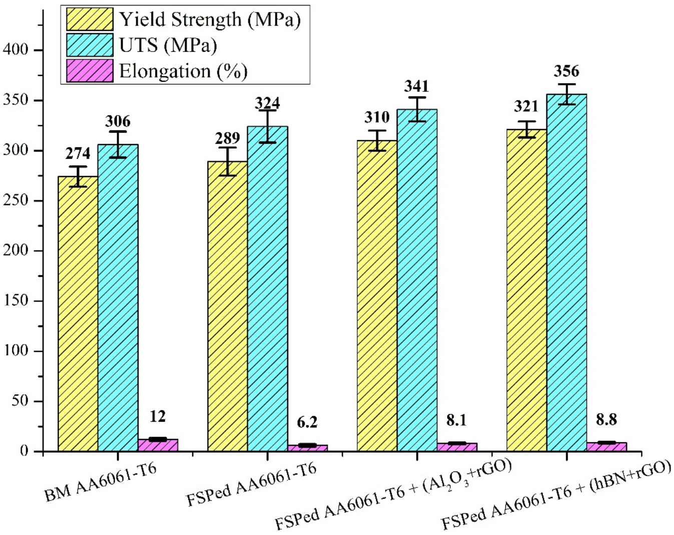

Fig. 7. Tensile test results of all the samples

Fig. 8(a, b) depicts the fractography of the ruptured surfaces of the hybrid reinforced samples. The rupture occurred towards the direction of the HAZ as the microhardness was slowly reducing towards the BM region. We identified a shear plane exhibiting a cup-cone morphology at the peripheries of the cracked specimens. Both samples showed ductile failure with honeycomb dimples, where the size of the dimple was also closer in size when observed, like the grain sizes found in the specimens. This indicates the distinct cleavage and plastic deformation characteristics due to the evenly distributed reinforcing particles, and a finer grain structure achieved through effective material mixing in the FSP.

2.6. Impact strength analysis

The Charpy test was conducted successfully for all the samples, their results are displayed in Fig. 9. The impact toughness for the BM was observed as 18.6 ± 2.2 J, and the value of

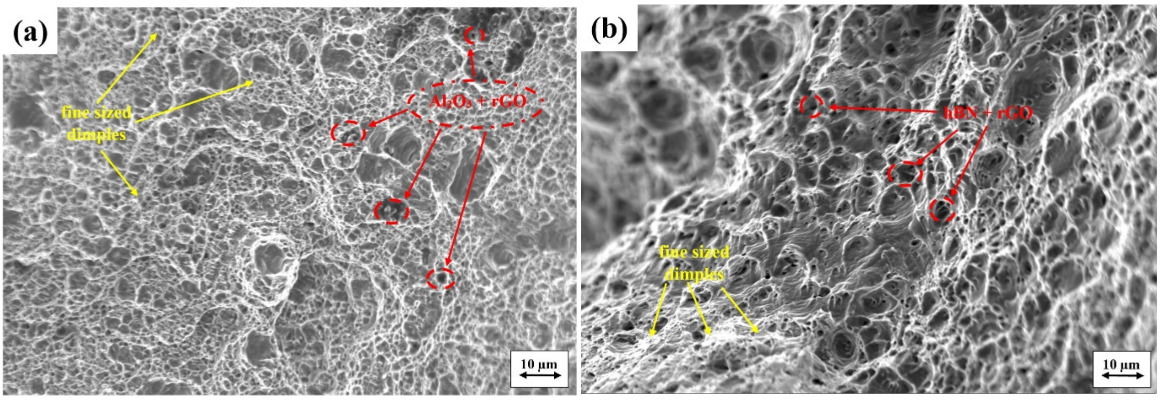

Fig. 8. Fractographies of the hybrid reinforced tensile samples: (a) AA6061-T6 + (Al_2O_3+rGO), (b) AA6061-T6 + (hBN+rGO)

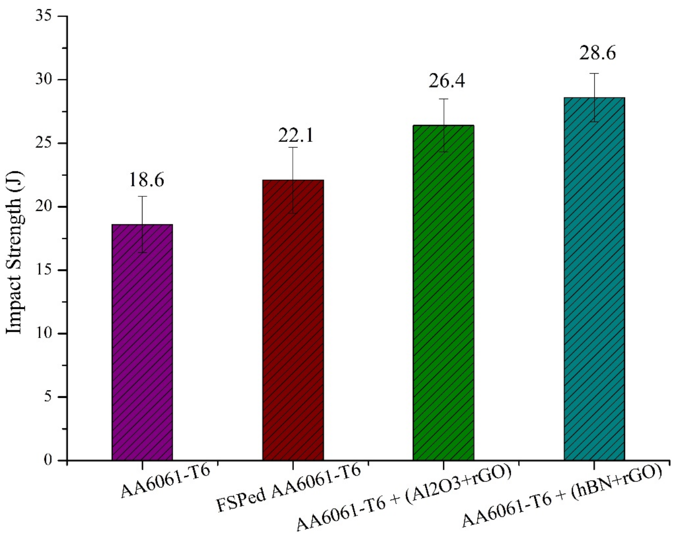

Fig. 9. Impact energies of all the samples

the FSPed sample without any reinforcement was observed as 22.1 ± 2.6 J. The FSPed specimens with the hybrid reinforcement (Al_2O_3 + rGO) was observed as 26.4 ± 2.1 J, and the hybrid reinforced (hBN+rGO) sample was observed as 28.6±1.9 J (53.76% increase compared to the BM). The reason for the improved impact toughness energy can be correlated with the grain size decrement and the ability of the reinforced particles which resist the crack propagation.

The SEM fractographies of the fractured impact test samples of the both hybrid reinforcement composite samples are displayed in Fig. 10(a, b), respectively. In contrast to the tensile specimens tested, the impact test causes the fracture to be shear-induced. Because plastic deformation occurs before fracture in hybrid reinforced samples, the fractured surfaces show finer dimples and tearing ridges in the failed impact test sample.

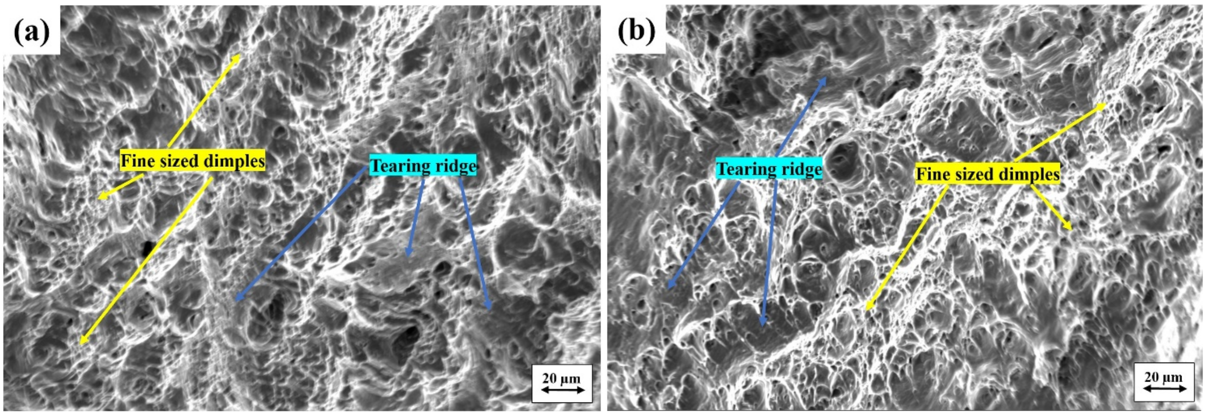

Fig. 10. Fractographies of the hybrid reinforced impact samples: (a) AA6061-T6 + (Al_2O_3+rGO), (b) AA6061-T6 + (hBN+rGO)

2.7. Microhardness profile

The graph in Fig. 11 shows the microhardness test results for different samples of BM AA6061-T6 alloy and hybrid reinforced samples after undergoing FSP. The microhardness (measured in Vickers Hardness) is plotted along the y-axis, while the distance (in mm) is plotted along the x-axis, which represents the cross-sectional distance across the processed region. The BM AA6061-T6 without any processing shows a relatively low and stable microhardness across the region, around 100-110 HV. FSPed AA6061-T6 line represents the material after FSP without any reinforcement. There is a slight increase in microhardness in the SZ, reaching about 140 HV. The microhardness of the hybrid reinforcement (AA6061-T6 + (Al_2O_3 + rGO)), increases significantly in the SZ, peaking at about 155 HV. The microhardness of the hybrid reinforcement (AA6061-T6 + (hBN + rGO)), increases significantly in the SZ, peaking at about 165-170 HV approximately. The addition of reinforcements such as (Al_2O_3 + rGO) and (hBN + rGO) to the AA6061-T6 alloy, combined with FSP significantly enhances the microhardness of the material. The highest microhardness was observed in the sample with (hBN + rGO) hybrid reinforcement. This indicates that the combination of these reinforcements effectively improves the mechanical properties of the alloy, making it more suitable for applications requiring higher hardness.

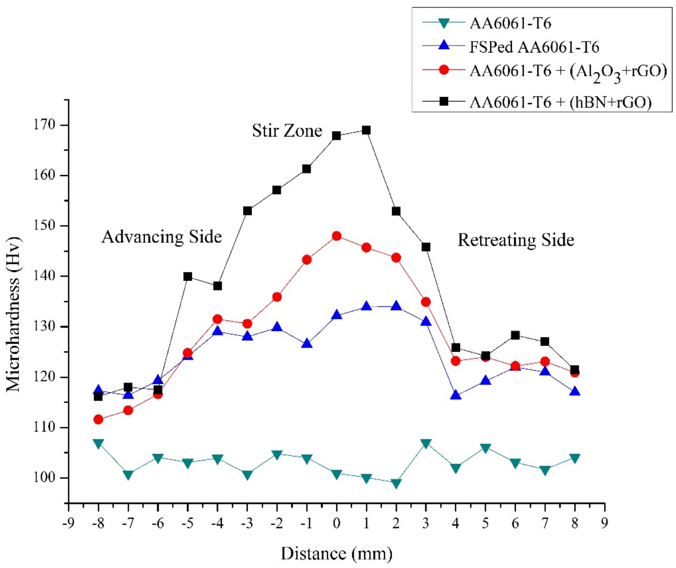

Fig. 11. Microhardness test results of all the samples

3. Conclusions

In the present work, AA6061-T6 was successfully reinforced with (Al_2O_3 + rGO) and (hBN + rGO) hybrid reinforcements via FSP with an aim to understand the comparison of microstructural, thermal conductivity and electrical conductivity changes, and an estimation of the improvement of mechanical properties for both the reinforcements.

From the results the following conclusions were made during the comparison study:

i. The hybrid composites (Al_2O_3 + rGO) obtained a grain size of 9.2 ± 4.5 µm and the composite (hBN + rGO) was measured as 8.7 ± 3.1 µm which was drastically reduced in comparison to the BM AA6061-T6 grain size of 84.2 ± 29.5 µm.
ii. Across the FSPed samples, by using XRD the peaks are almost identified for the base Al along with the reinforcements in the fabricated surface MMCs.
iii. The composite material AA6061-T6 + (Al_2O_3 + rGO), had the highest level of electrical conductivity, measuring around 2.1 × 107 S/m compared to the composite material AA6061-T6 + (hBN + rGO) having a little less electrical conductivity, measuring around 1.925×10^7 S/m.
iv. The composite material AA6061-T6 + (Al_2O_3 + rGO), had the highest level of thermal conductivity, measuring around 148 W/mK compared to the composite material AA6061-T6 + (hBN + rGO) having a little less thermal conductivity, measuring around 142 W/mK.
v. The composite material AA6061-T6 + (Al_2O_3 + rGO), had the highest UTS, measuring around 356 MPa compared to the composite material AA6061-T6 + (hBN + rGO) having a little less UTS, measuring around 341 MPa. Enhanced strength can be indirectly attributed to plastic deformation, particularly grain refinement.

vi. The composite material AA6061-T6 + (Al_2O_3 + rGO), had the highest impact strength, measuring around 28.6 J compared to the composite material AA6061-T6 + (hBN + rGO) having a less 26.4 J, measuring around 26.4 J.

vii. The composite material AA6061-T6 + (Al_2O_3 + rGO), had the highest microhardness, measuring around 170 Hv compared to the composite material AA6061-T6 + (hBN + rGO) having a less microhardness, measuring around 148 Hv. Reduced grain size reduces dislocation movement, resulting in improved strength and hardness.

REFERENCES

[1] Xiaohan You, Zhiquan Xing et al., Dev. Built. Environ., (2024). DOI: https://doi.org/10.1016/j.dibe.2023.100319

[2] M.Y. Khalid, R. Umer and K.A. Khan, Results Eng., (2023). DOI: https://doi.org/10.1016/j.rineng.2023.101372

[3] D. Varshney, K. Kumar, Ain Shams Eng. J., (2021). DOI: https://doi.org/10.1016/j.asej.2020.05.013

[4] S.C. Kundurti, A. Sharma, P. Tambe, A. Kumar, Mater. Today: Proc. **56** (3), 1468-1477 (2022). DOI: https://doi.org/10.1016/j.matpr.2021.12.337

[5] H. Pouraliakbar, M.R. Jandaghi et al., J. Alloys Compd., (2024). DOI: https://doi.org/10.1016/j.jallcom.2024.175400

[6] B. Leszczyńska-Madej, M. Madej, A. Wąsik et al., Int. J. Adv. Manuf. Technol., (2024), DOI: https://doi.org/10.1007/s00170-024-14252-w

[7] S. Tiwari, R. Kesharwani et al., Mater. Today Commun., (2024). DOI: https://doi.org/10.1016/j.mtcomm.2024.109543

[8] J. Iwaszko, M. Sajed, J. Compos. Sci. **5** (12), 323 (2021). DOI: https://doi.org/10.3390/jcs5120323

[9] Z.Y. Ma, Metall. Mater. Trans. A. **39**, 642-658 (2008). DOI: https://doi.org/10.1007/s11661-007-9459-0

[10] V. Sharma, U. Prakash, B.M. Kumar, J. Mater. Process. Technol. **224**, 117-134 (2015). DOI: https://doi.org/10.1016/j.jmatprotec.2015.04.019

[11] K. Li, X. Liu, Y. Zhao, Coatings. **9** (2), 129 (2019). DOI: https://doi.org/10.3390/coatings9020129

[12] S. A. Kasgari, M.R.M. Aliha et al., Mech. Compos. Mater, (2024). DOI: https://doi.org/10.1007/s11029-023-10158-y

[13] M.K. Abbassa, N.A.B. Sharhana, J. Mater. Eng, (2023). DOI: https://doi.org/10.61552/JME.2023.04.002

[14] M.A. Ammal and J. Sudha., Proc. Inst. Mech. Eng., Part B, (2022). DOI: https://doi.org/10.1177/09544054221126942

[15] M. Yunus, R. Alfattani, Coatings., (2023). DOI: https://doi.org/10.3390/coatings13091653

[16] D.K. Sharma, V. Patel et al., Materialwiss. Werkstofftech, (2020). DOI: https://doi.org/10.1002/mawe.202000130

[17] E.G. Mengstie, R.G. Rengiah et al., Discover Applied Sciences **6** (10), 493 (2024). DOI: https://doi.org/10.1007/s42452-024-06210-8

[18] S. Suman, S. Durjyodhan et al., Silicon **16** (5), 2219-31 (2024). DOI: https://doi.org/10.1007/s12633-023-02827-3

[19] M.S. Alia, I.Q. Al Saffar, Tribol. Ind., (2022). DOI: https://doi.org/10.24874/ti.1312.05.22.09

[20] E.R. Mahmoud, M. Takahashi, T. Shibayanagi, K. Ikeuchi, Wear. **268** (9-10), 1111-1121 (2010). DOI: https://doi.org/10.1016/j.wear.2010.01.005

[21] E.R. Mahmoud, M. Takahashi, T. Shibayanagi, K. Ikeuchi, Mater. Trans. **50** (7), 1824-1831 (2009). DOI: https://doi.org/10.2320/matertrans.M2009092

[22] M.D. Kannan, S.C. Kundurti et al., Mater. Today: Proc., (2024), DOI: https://doi.org/10.1016/j.matpr.2023.10.113

[23] N.A. Patil, S.R. Pedapati, O.B. Mamat, Arch. Metall. Mater. **65** (1), 441-457 (2020). DOI: http://dx.doi.org/10.24425/amm.2020.131747

[24] N.A. Patil, S.R. Pedapati, O.B. Mamat, A.M. Hidayat Syah Lubis, Coatings. **10** (6), 541 (2020). DOI: https://doi.org/10.3390/coatings10060541

[25] S.C. Kundurti, V.S. Aditya Mocherla, A. Sharma, R.S. Buradagunta, S. Goel, J. Mines Met. Fuels **71** (9), 1271-1285 (2023). DOI: https://doi.org/10.18311/jmmf/2023/35454

[26] S. Thanikodi, A.S. Britto, V.S. Dattu, S. Al Obaid, S. Alfarraj, M.A. Kalam, Int. J. Adv. Manuf. Technol., (2023). DOI: https://doi.org/10.1007/s00170-023-12198-z

[27] S.C. Kundurti, A. Sharma, Mater. Res. **26**, (2023). DOI: https://doi.org/10.1590/1980-5373-MR-2023-0176

[28] International A: ASTM E3-95 - Standard Practice for Preparation of Metallographic Specimens. (2017). Accessed.

[29] K.K. Jha, R.K Murshid Imam, Mater. Today: Proc., (2022). DOI: https://doi.org/10.1016/j.matpr.2022.02.262

[30] S.R. Manu Srivastava, S. Maheshwari et al., Crit. Rev. Solid State Mater. Sci, (2019). DOI: http://dx.doi.org/10.1080/10408436.2018.1490250

[31] International A: ASTM WK49229 – Standard Guide for Orientation and Location Dependence Mechanical Properties for Metal Additive Manufacturing. (2017). Accessed.

[32] International A. ASTM E92-17 – Standard Test Methods for Vickers Hardness and Knoop Hardness of Metallic Materials. West Conshohocken, PA, USA: ASTM International; 2017.